AD-A170 488 MODELING OF INFILTRATION KINETICS AND INTERFACIAL BOND STRENGTH IN ALUMIN (U) COLORADO SCHOOL OF MINES GOLDEN CENTER FOR WELDING RESEARCH G R EDWARDS ET AL. 1986 1/1

UNCLASSIFIED SSM-MT-CWR-023 N00014-85-K-0451 F/G 11/6 NL

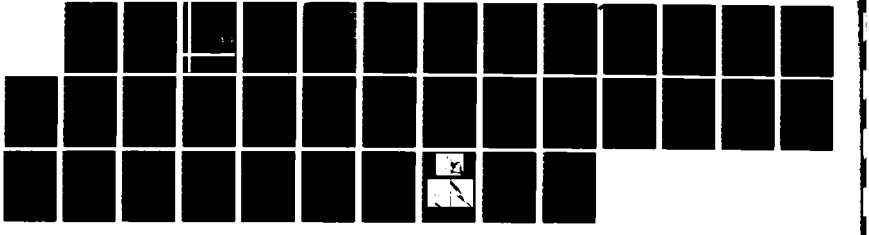

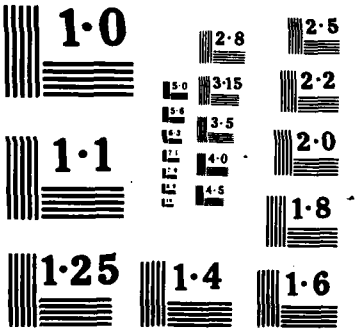
1·0
1·1
1·25
1·4
1·6
1·8
2·0
2·2
2·5
2·8
3·15
3·5
4·0
4·5
5·0

AD-A170 480

(12)

MT-CWR-086-023

MODELING OF INFILTRATION KINETICS AND INTERFACIAL BOND STRENGTH IN ALUMINUM MATRIX-SILICON CARBIDE COMPOSITES

ANNUAL REPORT

(May 1, 1985 to April 30, 1986)

by:

G.R. Edwards, D.L. Olson, G.P. Martins
B.R. Lanning and P.B. Maxwell

Center for Welding Research
Colorado School of Mines
Golden, Colorado 80401

Submitted to:

Dr. Steven G. Fishman
Scientific Officer
Materials Division
Office of Naval Research
800 N. Quincy Street
Arlington, VA 22217

Contract N00014-85-K-0451

CSM

Department of Metallurgical Engineering
Colorado School of Mines
Golden, Colorado 80401

MT-CWR-086-023

MODELING OF INFILTRATION KINETICS AND INTERFACIAL BOND STRENGTH IN ALUMINUM MATRIX-SILICON CARBIDE COMPOSITES

ANNUAL REPORT

(May 1, 1985 to April 30, 1986)

by:

G.R. Edwards, D.L. Olson, G.P. Martins
B.R. Lanning and P.B. Maxwell

Center for Welding Research
Colorado School of Mines
Golden, Colorado 80401

Submitted to:

Dr. Steven G. Fishman
Scientific Officer
Materials Division
Office of Naval Research
800 N. Quincy Street
Arlington, VA 22217

TABLE OF CONTENTS

INFILTRATION KINETICS AND INTERFACIAL BOND STRENGTH IN ALUMINUM MATRIX-SiC COMPOSITES

INTRODUCTION

The objective in this research is to gain a fundamental understanding of the wetting and adhesion of aluminum alloys to SiC. The preliminary approach has been to study the infiltration kinetics of molten aluminum alloys into green silicon carbide compacts and relate the results to the interfacial bond strength. Since both infiltration rate and interfacial bond strength are related to the interfacial tension at the interface, our approach has been to isolate those parameters which affect both infiltration kinetics (i.e. viscosity, density, and pore size) and interfacial bond strength (i.e. enthalpies of solution and electronic contributions) and then to correlate the kinetics and bond strength to the most fundamental parameters.

EXPERIMENTAL APPROACH AND RESULTS

Infiltration Kinetics

The kinetics of infiltration are being studied by the technique of capillary rise. Infiltration rates can be determined by measuring the height of infiltration of molten aluminum in both green compacts and fine-bore capillaries of CVD silicon carbide as a function of time. A schematic diagram is shown in Figure 1.

The body and surface forces acting on the liquid column in a vertical capillary, including the meniscus, are shown in Figure 2. The upward force of the surface tension and the downward forces due to "end-drag effects", viscous resistance and gravity sum vectorially, and are equated to the inertial acceleration of the liquid column, as shown in Equation 1:

$$\Sigma F = F_{\gamma} + F_{g} + F_{\eta} + F_{ed} = \frac{d}{dt}\left(m(t)\frac{dh}{dt}\right) \qquad (1)$$

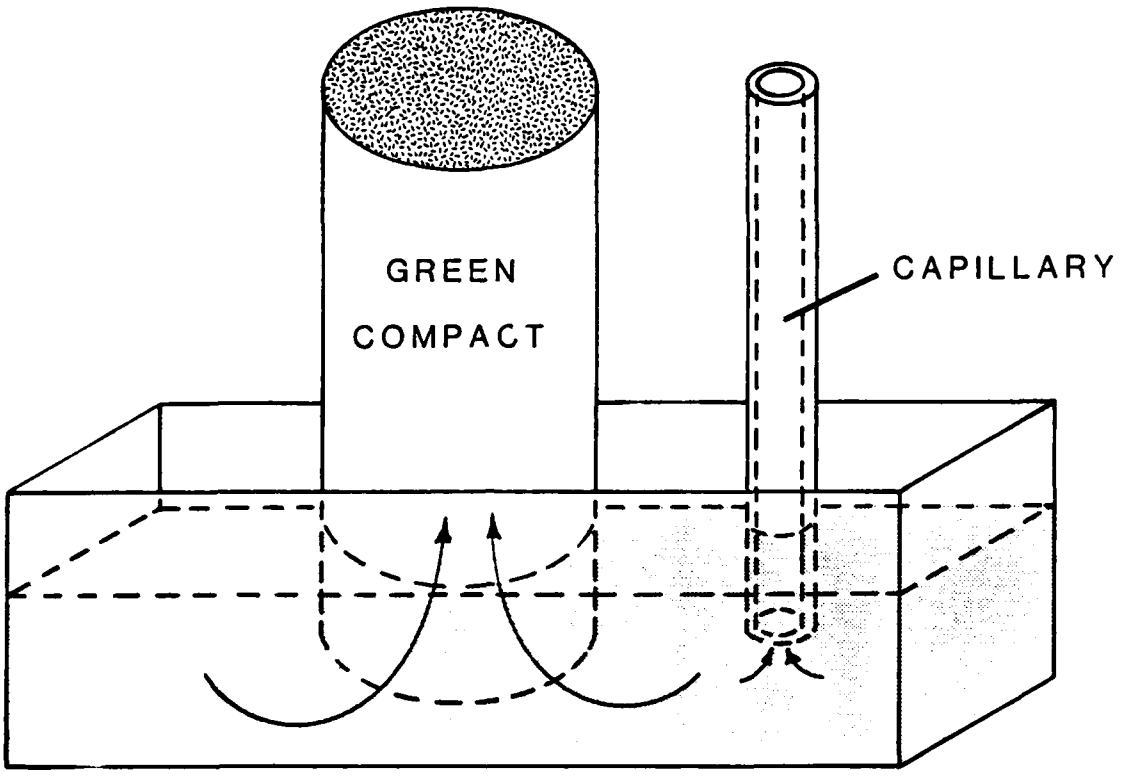

Figure 1. Conceptual scheme of infiltration studies.

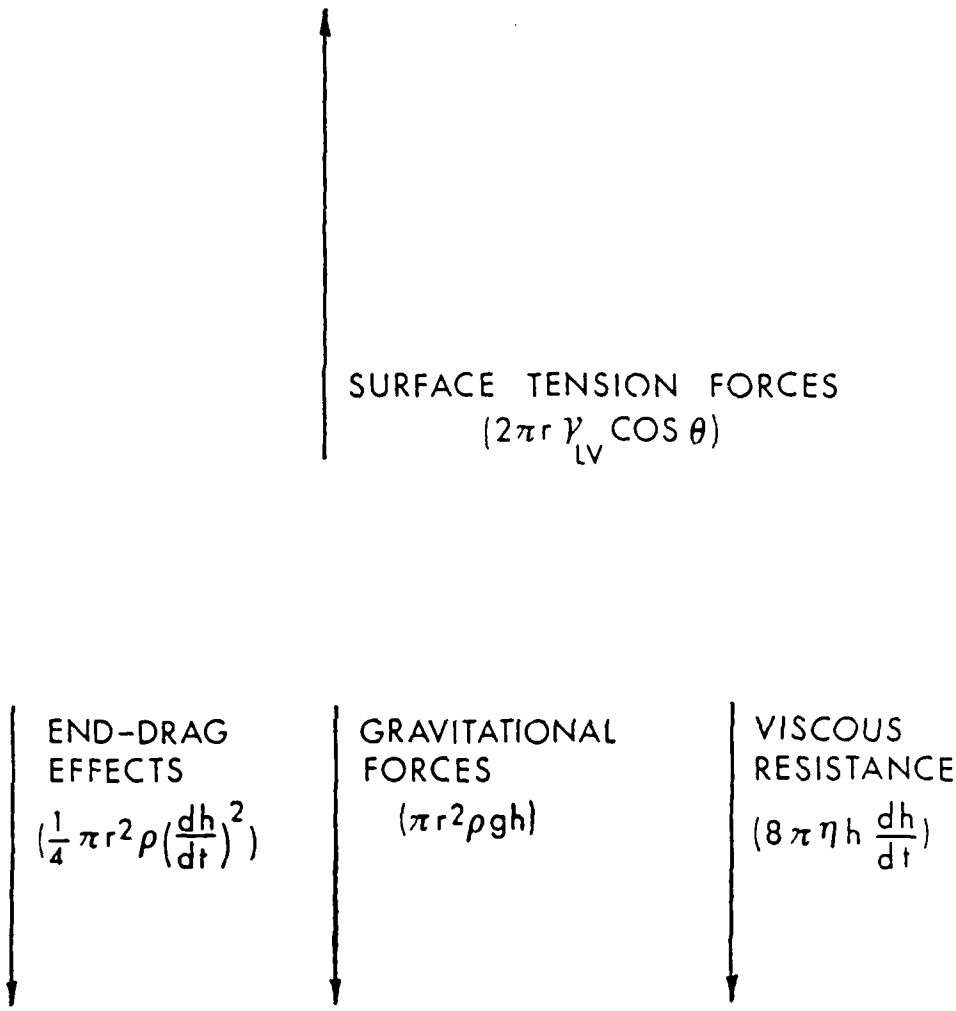

Figure 2. Schematic of forces acting in a cylindrical capillary.

An Approximate Solution:

From equation 1, a relation can then be derived which relates infiltration rate to viscosity, density, surface tension and contact angle of the liquid and pore radius of the capillary. The expanded form of the equation is given as:

$$2\pi r\, \gamma_{LV} \cos\theta - \pi r^2 \rho\, gh - 8\pi\eta h \frac{dh}{dt} - \frac{1}{4} \pi r^2 \rho \left(\frac{dh}{dt}\right)^2 = \pi r^2 \rho \frac{d}{dt}\left(h \frac{dh}{dt}\right) \quad (2)$$

where

γ_{LV} = liquid-vapor surface energy (surface tension)

θ = liquid-solid contact angle

r = capillary radius

h = height of infiltration at time t

η = viscosity of the liquid infiltrant

ρ = density of the liquid

g = gravitational constant

For conditions where shear forces predominate and end effects are neglected, the differential equation is reduced to:

$$h \frac{d^2h}{dt^2} + ah\frac{dh}{dt} + C = 0 \quad (3)$$

where:

$C = gh - b$

An approximate solution to the differential equation can be found and the result is given by the following equation:

$$h^2 = \frac{\rho^2 r^4}{32\eta^2}\left[\frac{8\eta}{\rho r^2}\left(\frac{2\gamma_{LV}\cos\theta}{\rho r} - gh\right)t - \exp\left(\frac{-8\eta t}{\rho r^2}\right) + 1\right] \qquad (4)$$

Here, infiltration height is presented as a function of density, viscosity, surface tension, contact angle, and capillary radius.

For small fractions of infiltration (~20%) the time required is proportional to the square of the fraction infiltrated, and will be dependent on the properties of the liquid; i.e. viscosity, density, surface tension, and contact angle. By adding different solute elements to the liquid infiltrant and thereby altering the properties of the liquid, the corresponding time for infiltration should vary according to that predicted by Equation 4. A diagram of this concept is shown schematically in Figure 3. Calculated values of experimental data are presented in Table 1 and Figure 4.

Parameters which Effect the Infiltration Kinetics:

In the previous section, Equation 4 was derived for the infiltration kinetics of a liquid into a porous solid medium. According to this equation, the height of rise for a liquid into a vertical column is primarily determined by 1) viscosity, 2) density, 3) pore size, and 4) surface tension and contact angle. The effect of each of these parameters on the infiltration kinetics will be discussed in more detail.

For most liquid metals, viscosity exhibits Arrhenius type behavior, and can be given by the following equation:

$$\eta V^{1/3} = A \cdot \exp\left[\frac{C}{V(T-T_m)}\right] \qquad (5)$$

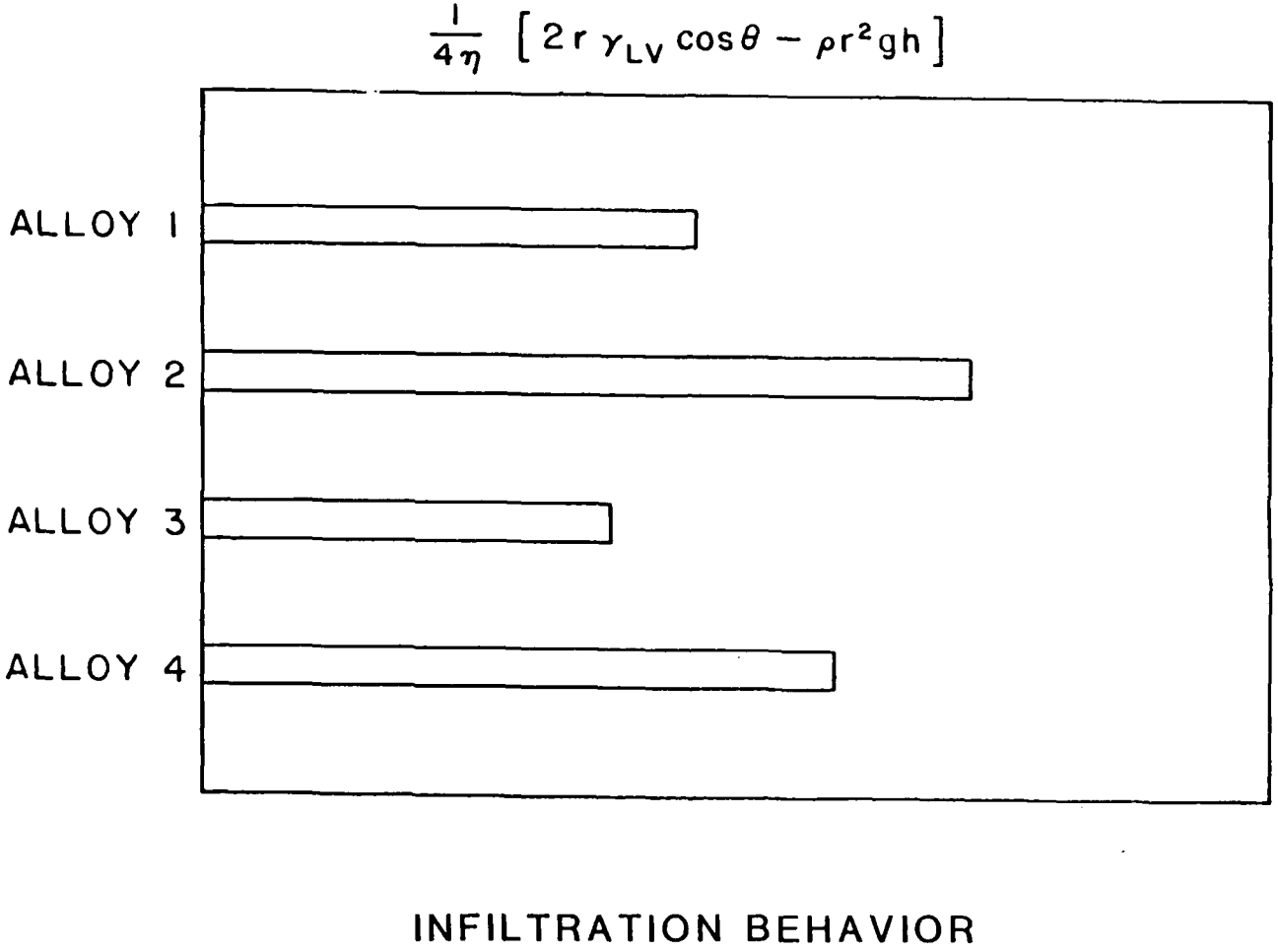

Figure 3. Qualitative effect of solute addition to infiltrant.

Table 1. Infiltration of SiC compacts with aluminum alloys at 1000 C (calculated from the infiltration equation).

ALLOY	PHYSICAL PROPERTIES					
	$\rho \times 10^{-3}$ ($Kg \cdot m^{-3}$)	$\eta \times 10^{3}$ ($Kg \cdot m^{-1} s^{-1}$)	γ ($Kg \cdot s^{-2}$)	θ^{o}	H_{max} (m)	$t_{h=0.1m}$ (s)
PURE ALUMINUM	2.28	0.80	0.82	50	4.7	3.1
Al-2% Cu	2.31	0.79	0.81	50	4.6	3.1
Al-4% Cu	2.35	0.80	0.81	50	4.5	3.1
Al-1% Mg	2.29	0.80	0.78	50	4.5	3.3
Al-3% Mg	2.27	0.81	0.69	50	4.0	3.7
Al-2.6% Cu -0.13%Zr -1.8% Li	1.98	1.04	0.42	50	2.8	8.0
Al-1,5% Cu-1% Mg -0.13%Zr -2.5% Li	1.92	1.33	0.33	50	2.3	13.1

REFERENCES:

1. BATELLE REPORT FOR ALCOA TECHNICAL CENTER, CONTRACT 2311206478, 1984
2. E. GEBHART AND K. DETERING, Z. Metallk., Vol. 50, 1959, p 379-385
3. E. GEBHART, M. BECKER AND S. DORNER, Aluminium, Vol. 31, 1955, p 315-321
4. G. LANG, Aluminium, Vol. 49, 1973, p 231-238
5. G. LANG, Aluminium, Vol. 50, 1974, p 731-734
6. R. WARREN AND C-H ANDERSSON, Composites, Vol. 5, 1984, p 101-111

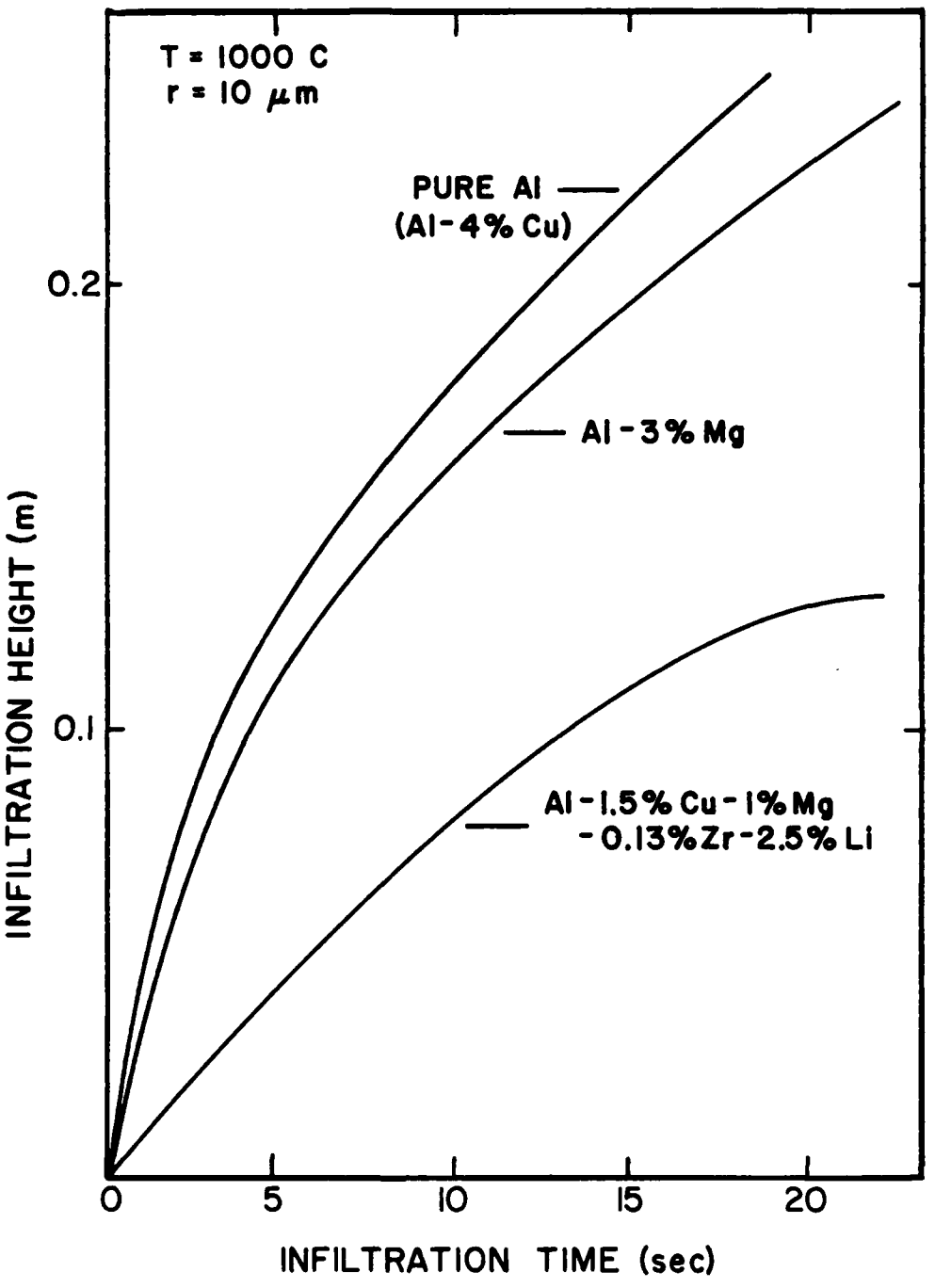

Figure 4. Infiltration height as a function of time for three different aluminum alloys in SiC compacts.

where:

A,C = Constants

V = Specific Volume

$(T-T_m)$ = Superheat

Although not apparent from the equation, viscosity is related to density through the exponential term, $A/V^{1/3}$ (written in units of viscosity). The effects of silicon, copper, and magnesium additions on the viscosity of aluminum are shown in Figure 5. Therefore, as the viscosity decreases, the height of infitration will increase.

The liquid-vapor surface tension is important to the infiltration rate. Temperature, alloy type, and alloy composition are all factors which will effect both the surface tension and the contact angle. As temperature increases surface tension decreases according to:

$$\gamma_{LV} = A - B(T - T_m) \qquad (6)$$

where:

A,B = Constants

$(T-T_m)$ = Superheat

The effect of alloying with silicon, copper, magnesium or lithium on the surface tension of aluminum is graphically illustrated in Figure 6.

As previously shown in Equation 3 for large times, the infiltration height can be maximized by decreasing the density. Density will also indirectly affect the viscosity (i.e., as the density decreases, the viscosity is also expected to decrease).

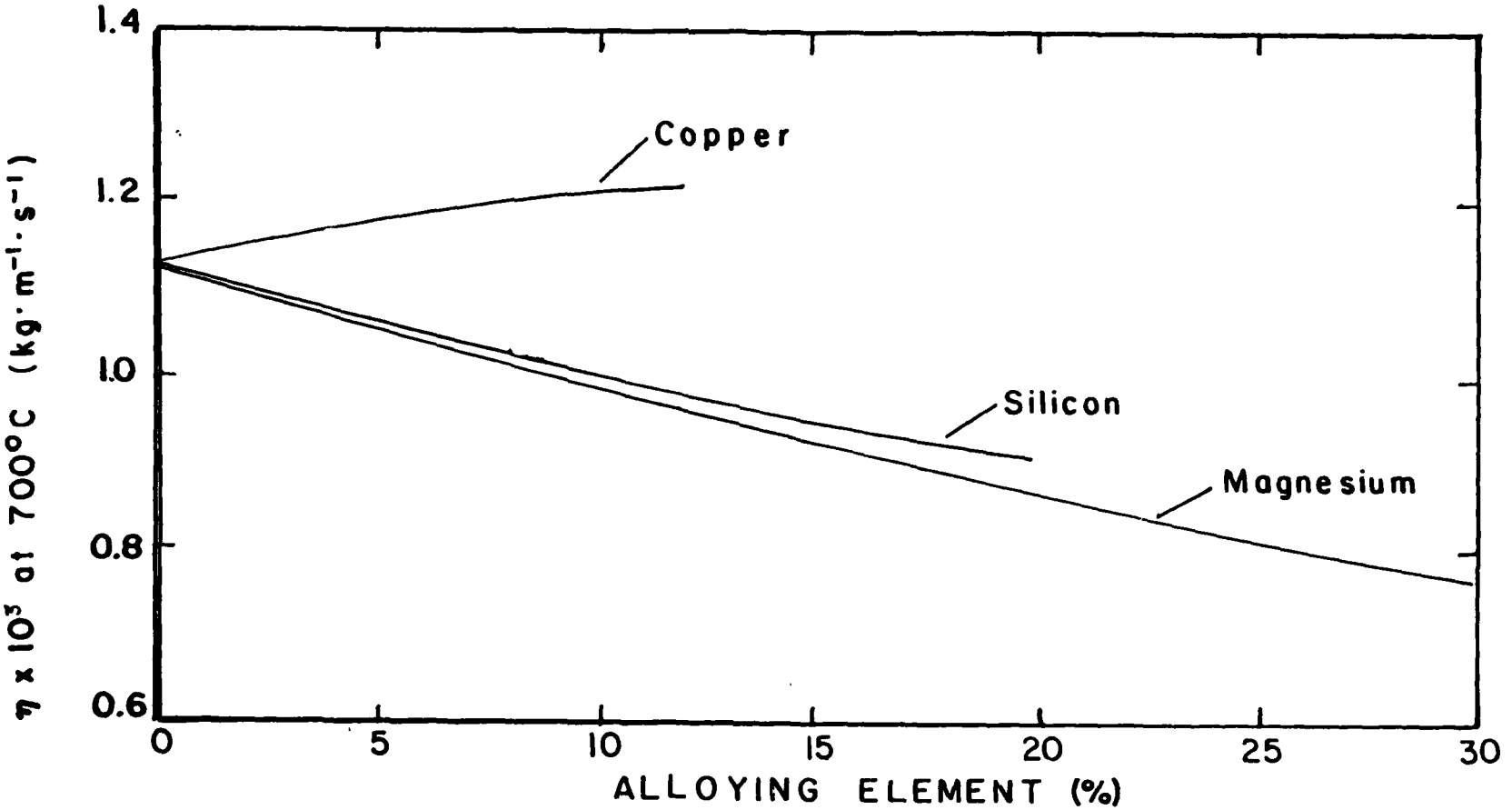

References:
1. E. Gebhardt, M. Becker and S. Dorner, Aluminium, Vol. 31, 1955, p 315 - 321
2. E. Gebhardt and K. Detering, Z. Metallk., Vol. 50, 1959, p 379 - 385

Figure 5. Effect of alloying additions on the viscosity of aluminum.

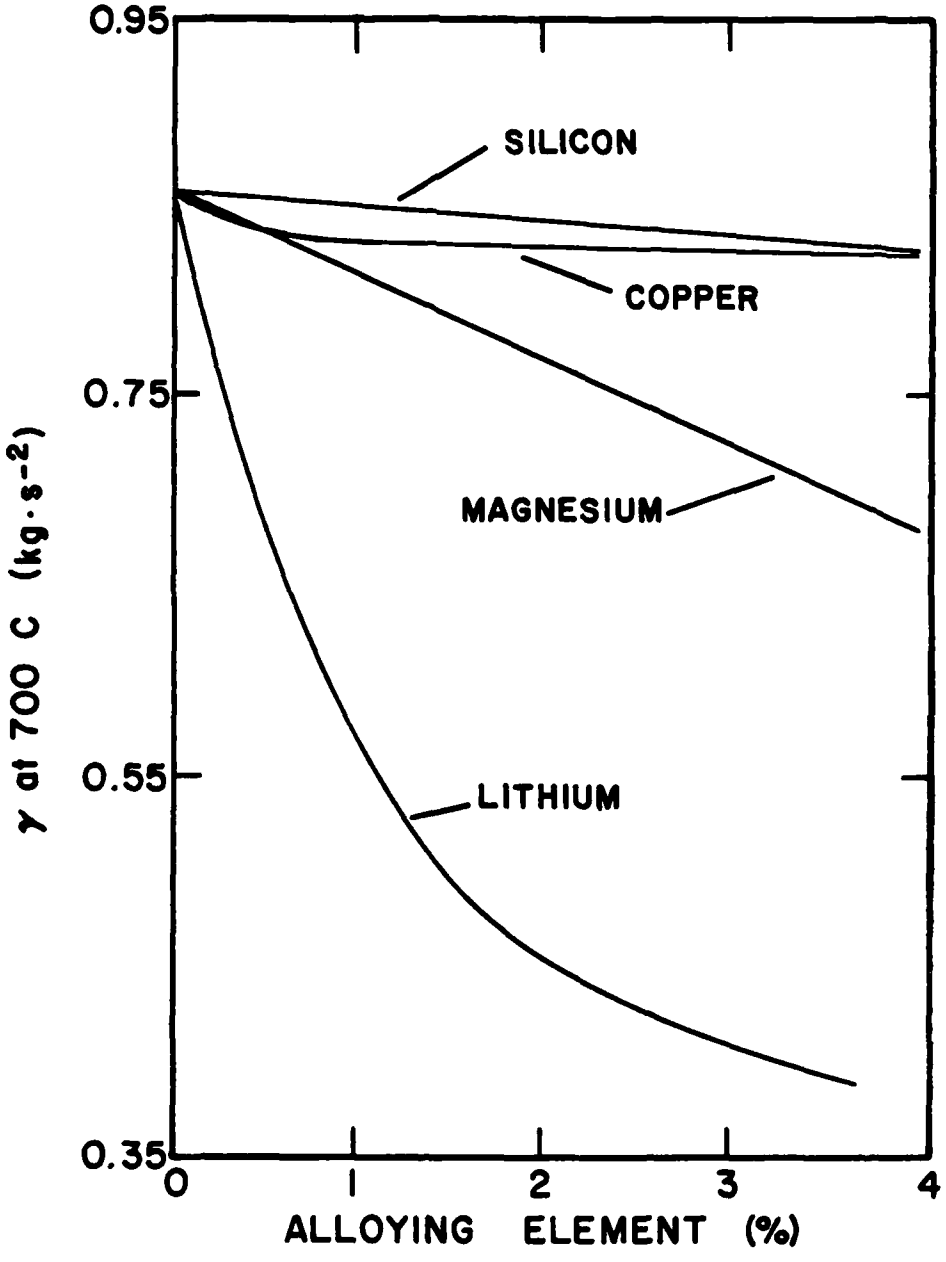

References:
1. G.Lang, Aluminum, Vol. 49, 1973, p. 231 - 238
2. G.Lang, Aluminum, Vol. 50, 1974, p. 731 - 734

Figure 6. Effect of alloying additions on the surface tension of aluminum.

During the initial stages of infiltration of liquid metals into powder compacts, infiltration rate decreases as the powder size increases. This is consistent with the observation that as the pore size decreases, the restraining force due to gravity decreases and that due to viscosity increases. Infiltration rate is also affected by the shape of the pore. As the presintering time for a metal powder compact increases and the pore shape becomes less angular and more rounded, the rate of infiltration is expected to increase.

Alternate Approach Using Dimensional Analysis:

An alternate approach, using characteristic dimensionless quantities, was also considered to analyze infiltration of a compact by liquid metal. Recalling the general infiltration kinetics equation:

$$h \frac{d^2h}{dt^2} + \frac{5}{4} \left(\frac{dh}{dt}\right)^2 + ah \frac{dh}{dt} + gh = b \qquad (7)$$

where:

$$a = \frac{8\eta}{\rho r^2}$$

$$b = \frac{2\gamma_{LV}\cos\theta}{\rho r}$$

Establishing dimensionless quantities, the resulting normalized expression is given by:

$$\xi \frac{d^2\xi}{d\tau^2} + \frac{5}{4} \left(\frac{d\xi}{d\tau}\right)^2 + \lambda \xi \frac{d\xi}{d\tau} + \xi = 1 \qquad (8)$$

where:

$$\lambda = \left(\frac{ab^{1/2}}{g}\right)$$

$$\tau = \left(\frac{g}{b^{1/2}}\right) t$$

$$\xi = \left(\frac{h}{H_s}\right); \text{ where } H_s = \frac{b}{g}$$

In this instance, the parameters of the equation are normalized to obtain dimensionless groups characteristic of the infiltration kinetics. The dimensionless group λ incorporates the effects of viscosity and interfacial tension into one variable.

The equation was solved numerically using a digital computer, and the results are shown in Figures 7 to 12 and Table 2. Two limiting asymptotic behaviors can be delineated. For λ less than 10^{-2} (inviscid system) the infiltration behavior is periodic as shown in Figure 7. In Figure 8, the time to infiltrate various fractions of pore volume is shown for this asymptotic case.

For λ greater than 10^{2} (viscous system) the infiltration behavior is shown in Figure 9. The behavior for this limiting system as predicted by the numerical solution is compared in Figure 10 with the asymptotic "short-time" solution shown previously. For infiltration fractions less than 20 percent, the error in the time for infiltration is less than one percent. The asymptotic behavior predicted by the numerical solution is shown in Figures 11 and 12; the limiting value of λ is delineated here.

Finally, the dimensionless parameters corresponding to a number of aluminum alloy systems in contact with a porous silicon carbide compact is shown in Table 2. It is apparent that the values of λ are larger than 100

$$\tau_1 = \beta_1 t; \quad \beta_1 = \frac{g}{b^{1/2}} = \frac{g(\rho r)^{1/2}}{(2\gamma \cos\theta)^{1/2}}$$

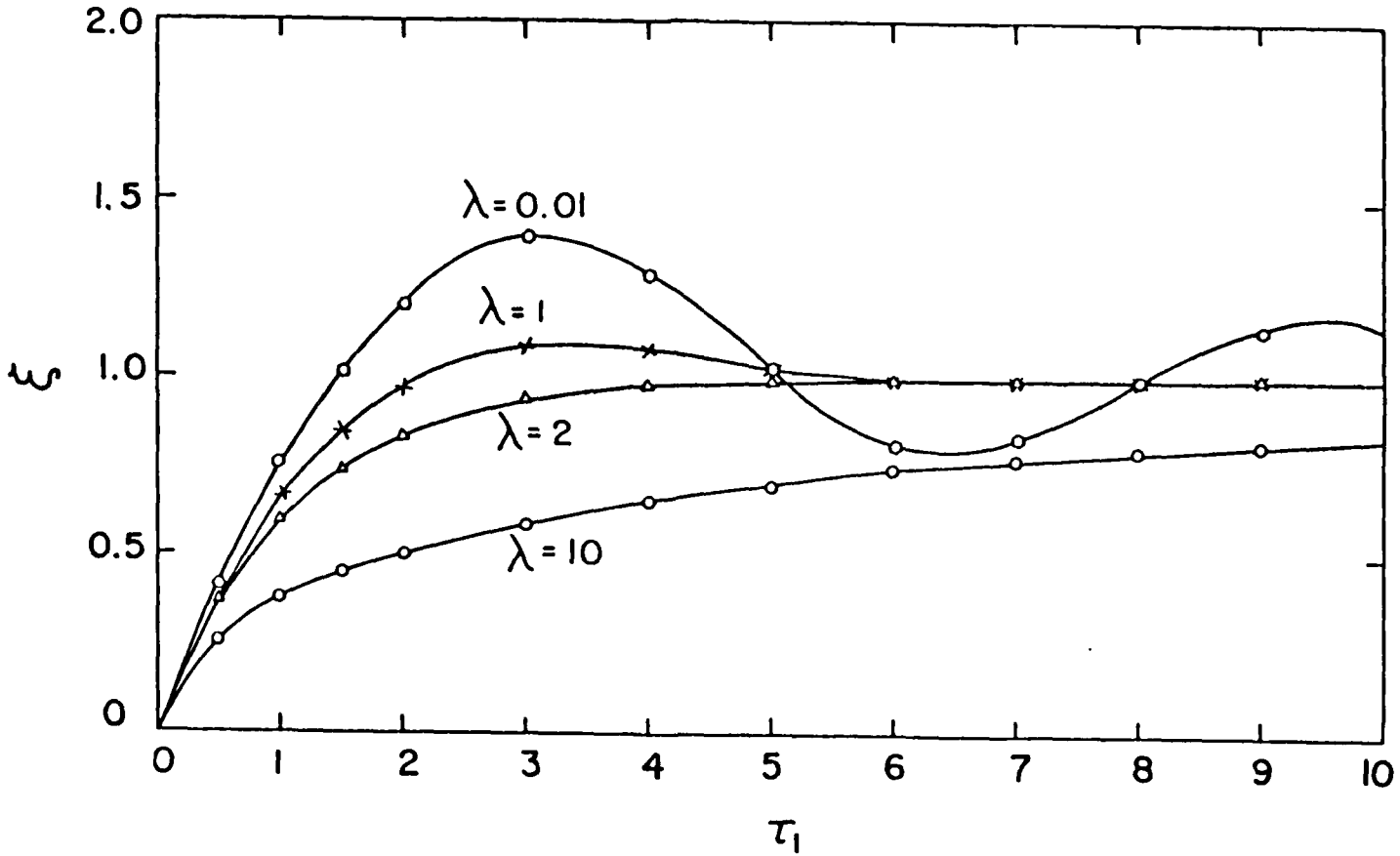

Figure 7. Fraction of pore volume infiltrated versus scaled dimensionless time, τ_1.

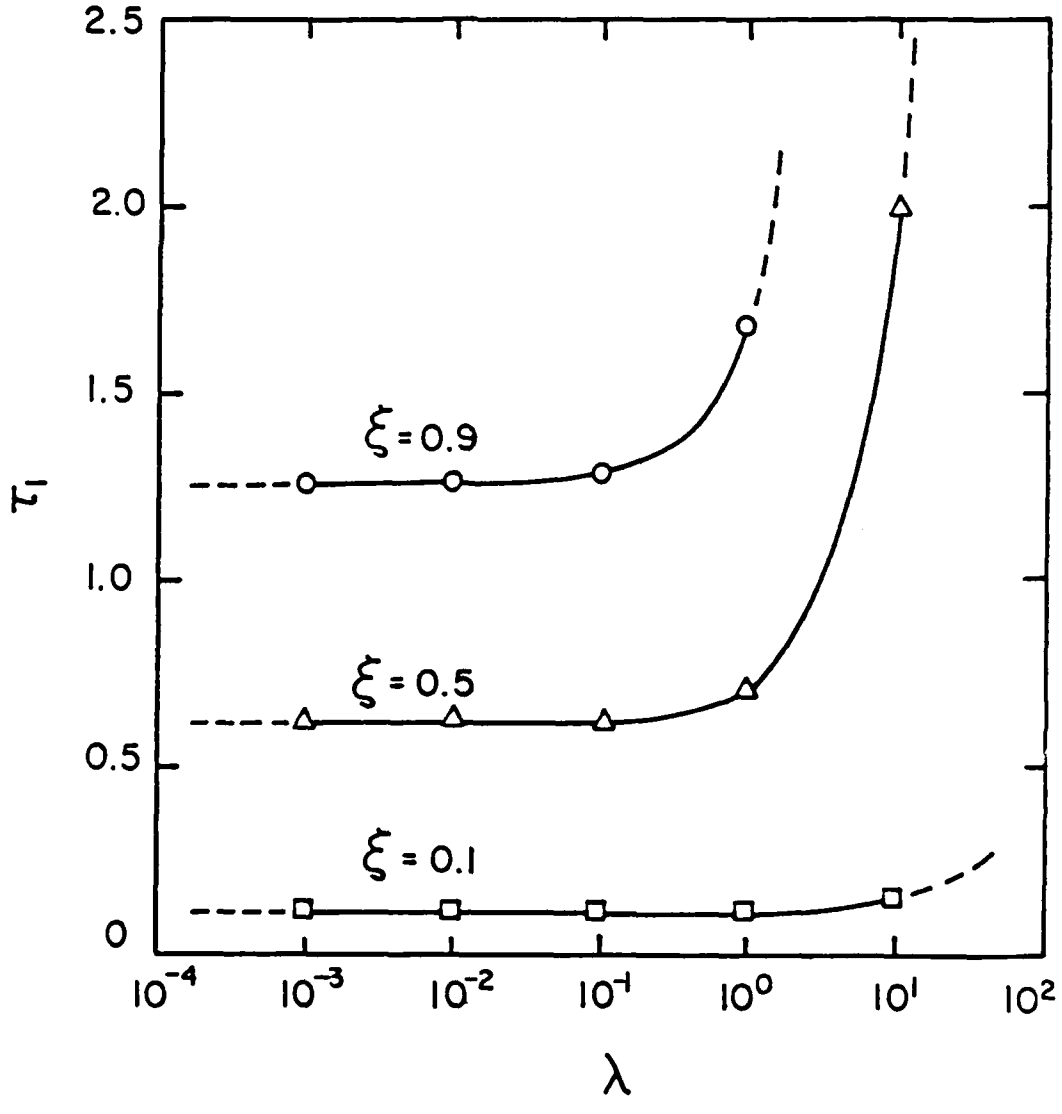

Figure 8. Asymptotic behavior of system for small values of λ ($<10^{-2}$) - (inviscid system).

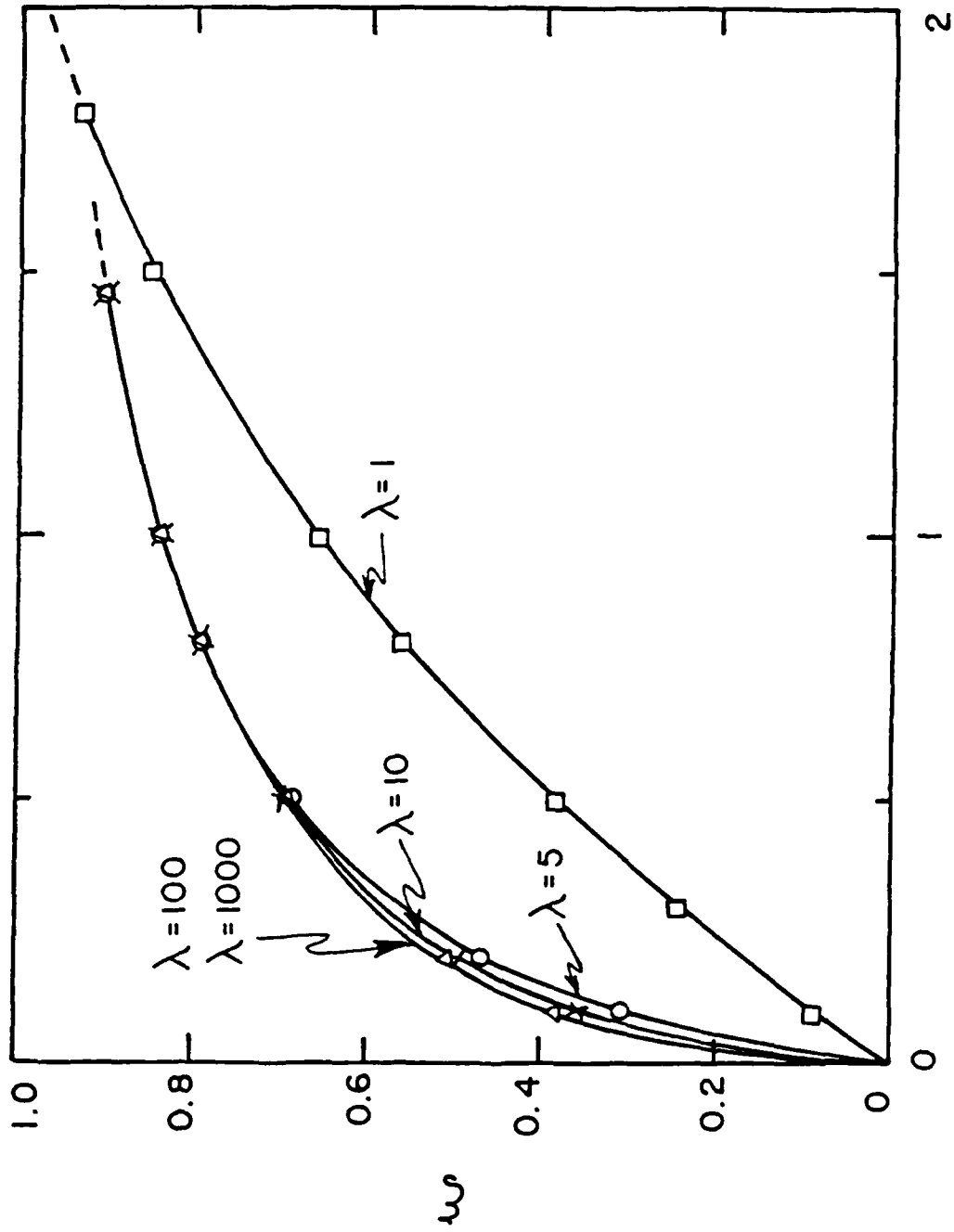

Figure 9. Fraction of pore volume infiltrated versus scaled dimensionless time, τ_2.

$$^{*}\tau_2 = \frac{1}{2}\left(\frac{\xi^2}{1-\xi}\right); \quad \lambda > 100$$

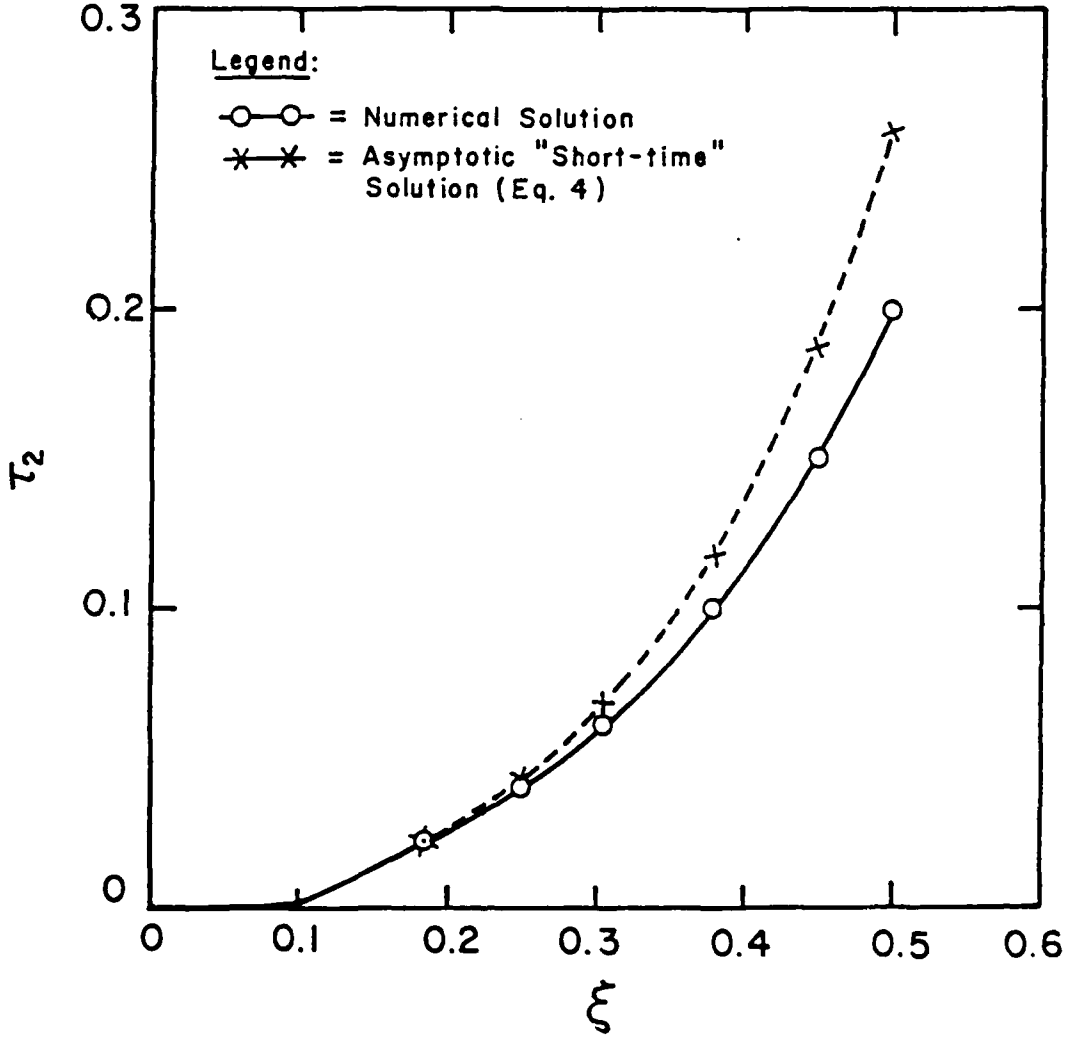

Figure 10. Scaled dimensionless time (τ_2) required to infiltrate a given fraction of pore volume. Asymptotic "short time" solution * is valid for up to 20% infiltration.

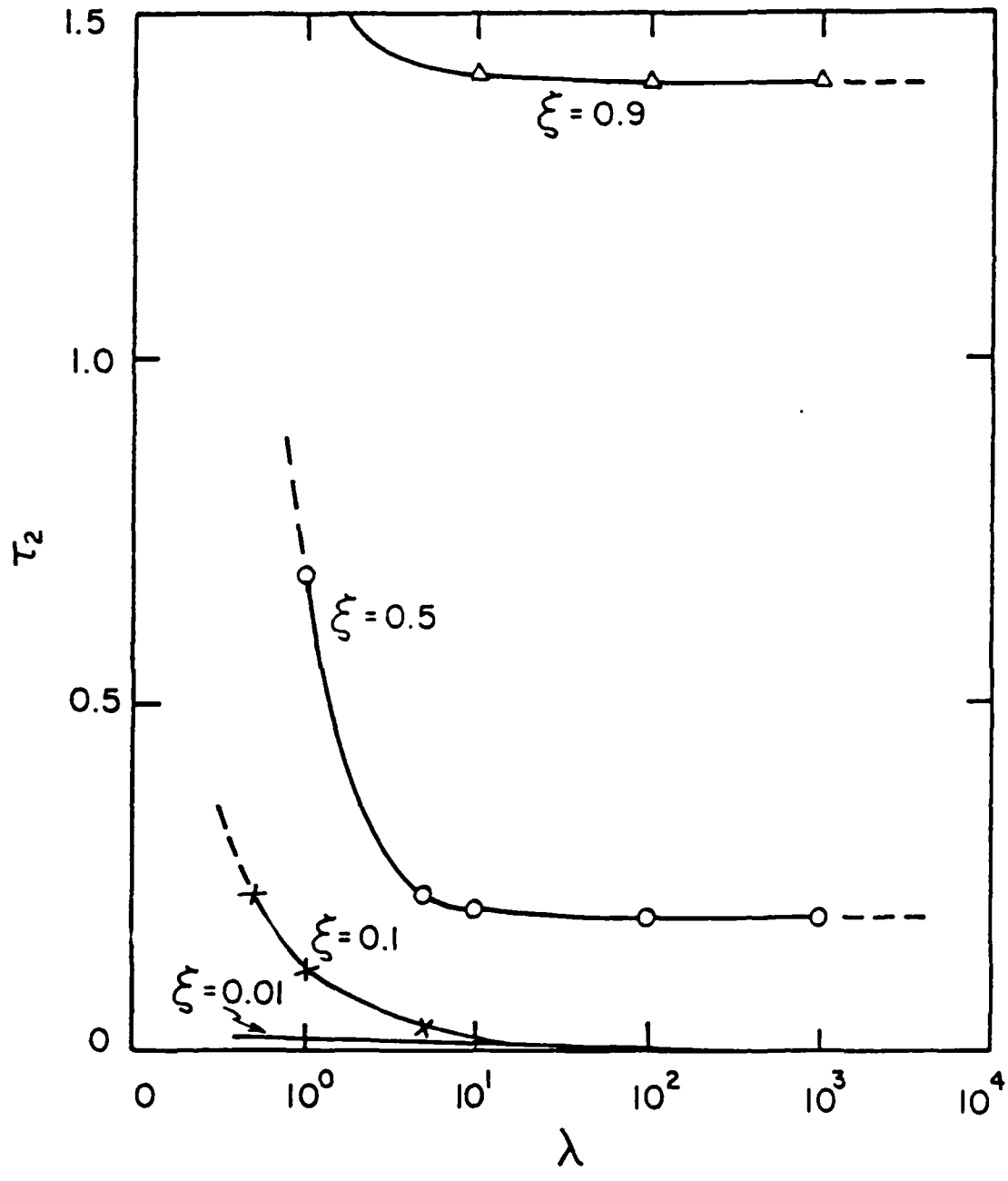

Figure 11. Asymptotic behavior of system for large values of λ ($>10^2$) - ("viscous system").

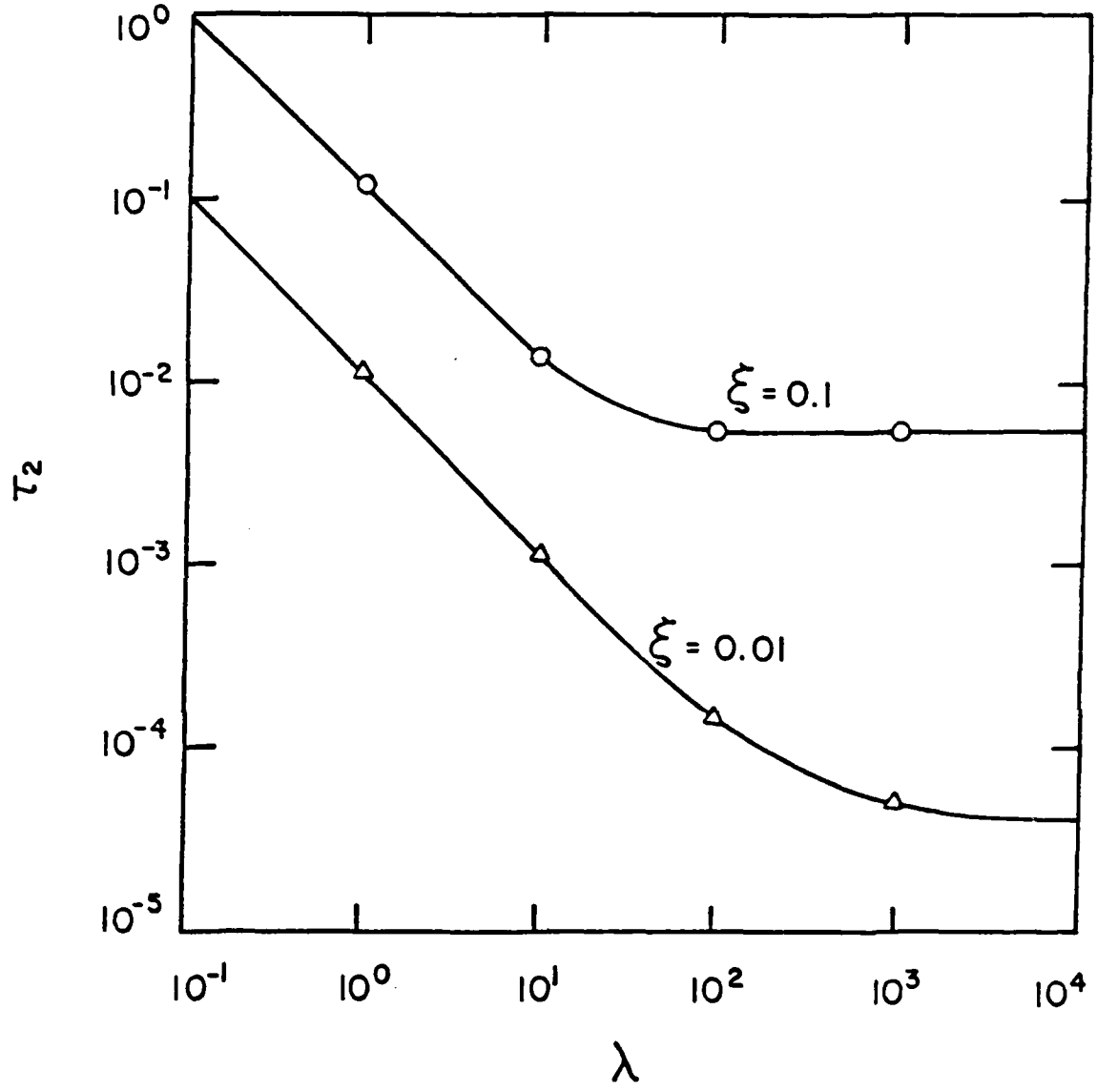

Figure 12. Asymptotic behavior of system for large values of λ (>10^2) - ("viscous system") expanded ordinate.

Table 2. Dimensionless parameters and real times for infiltration of SiC compacts with aluminum alloys at 1000C.

ALLOY	$\lambda \times 10^{-6}$		$b_2 \times 10^7$ (S^{-1})		$t_{\xi=2\%}$ (S)		$t_{\xi=5\%}$ (S)	
	r = 1 μm	r = 10 μm	r = 1 μm	r = 10 μm	r = 1 μm	r = 10 μm	r = 1 μm	r = 10 μm
AL	6.15	0.0195	0.741	741	2750	2.75	17800	17.8
AL-2% Cu	5.92	0.0187	0.780	780	2620	2.62	16900	16.9
AL-4% Cu	5.78	0.0183	0.816	816	2500	2.50	16100	16.1
AL-1% Mg	5.96	0.0189	0.786	786	2600	2.60	16700	16.7
AL-3% Mg	5.75	0.0182	0.863	863	2360	2.36	15200	15.2
AL-2.6% Cu 0.13% Zr-1.8% Li	7.07	0.0224	0.840	840	2430	2.43	15700	15.7
AL-1.5% Cu 1% Mg-0.13% Zr 2.5% Li	8.40	0.0226	0.786	786	2600	2.60	16700	16.7

and consequently the asymptotic behavior for large λ is appropriate to these systems. The times for two values of the volume-percents-infiltrated are also shown in this table, for two pore radii.

Interfacial Bond Strength

From electronic considerations, the interaction energy or bond strength between two materials can be related to the differences in the respective Fermi levels (i.e. the highest occupied energy state of an electron in a material) and to other physically significant quantities. When two materials are placed in electrical contact, electrons will flow in one direction until equilibrium is achieved and a potential, known as the contact potential, can be measured. (Hall measurements can also be used to correlate differences in the fermi levels). As the difference between Fermi levels increases, the contact potential and corresponding bond strength would also be expected to increase. In the case of the aluminum/silicon carbide system, doping SiC with phosphorous or alloying the liquid aluminum with lithium would be expected to increase the difference between the Fermi levels and increase the bond strength. Alloying with silicon would be expected to have a reverse effect. This concept is shown in Figure 13.

The next step is to relate the contact potential to the interfacial bond strength. Interfacial bond strength or the work of adhesion can be defined for two clean metals, A and B, in contact;

$$\gamma_{BOND}^{AB} = \gamma_{SV}^{A} + \gamma_{SV}^{B} - \gamma_{SS}^{AB} \qquad (9)$$

where S and V refer to the solid and vapor states respectively. Using the results from Miedema's theory of alloying, the interfacial energy between two

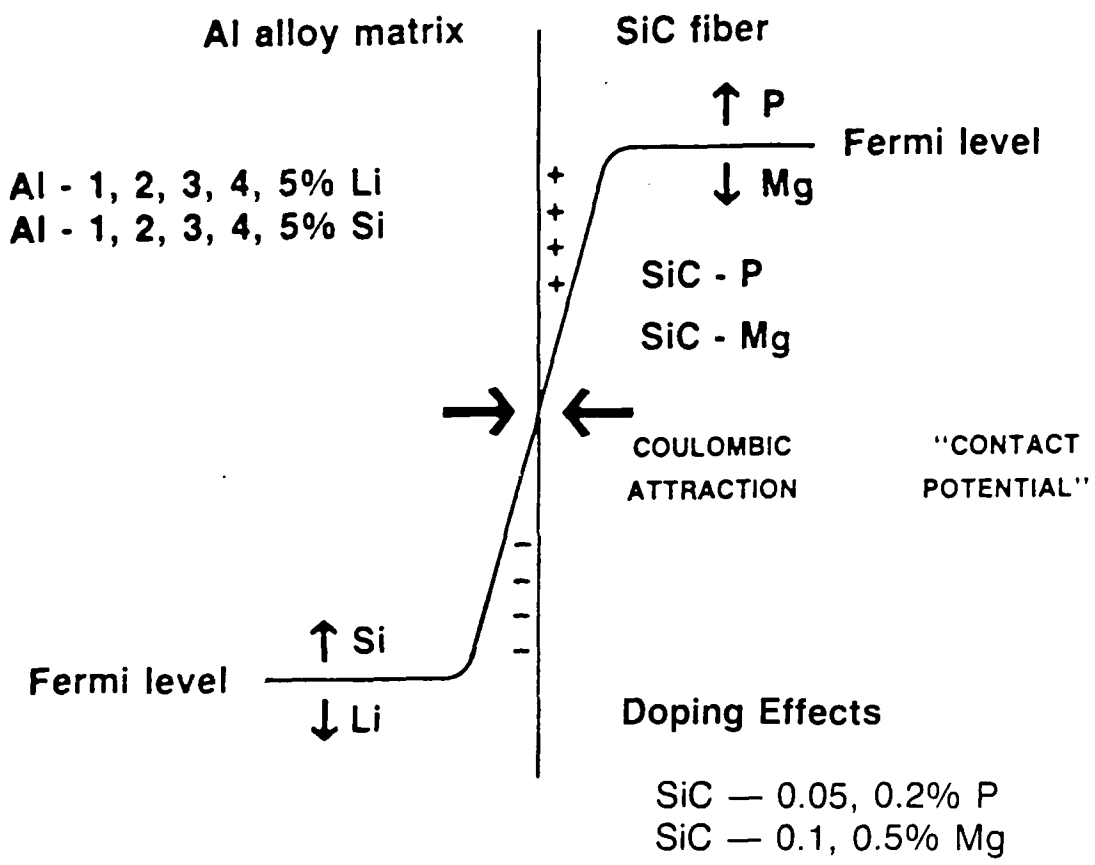

Figure 13. Conceptual experiment: Matrix or fiber alloying.

solid phases can be split into a surface energy term (GEOM) and a chemical term (CHEM).

$$\gamma_{SS}^{AB} = \gamma_{SS}^{GEOM} + \gamma_{SS}^{CHEM}$$
$$\gamma_{SS}^{GEOM} = 0.15\ (\gamma_{S,o}^{A} + \gamma_{S,o}^{B}) \qquad (10)$$

and

$$\gamma_{SS}^{CHEM} \propto \Delta H_f \sim [-Pe(\Delta\phi^*)^2 + Q_o\ (\Delta n_{ws}^{1/2})^2 - R]$$

where:

P, e, Q_o, R = Constants

$\Delta\phi^*$ = Electronegativity difference ($\propto$ to difference in work functions)

Δn_{ws} = Difference in electron density at Wigner-Seitz boundary ($\propto$ to difference in compressibilities)

The surface energy term is analogous to the energy of a grain boundary in a solid metal; the chemical term is related to the enthalpy of formation. An equation for the solid-solid interfacial energy is therefore given by:

$$\gamma_{SS}^{AB} = 0.15(\gamma_{S,o}^{A} + \gamma_{S,o}^{B}) + \gamma_{SS}^{CHEM} \qquad (11)$$

and a final form of the equation; which relates interfacial energies to bond strength, is given by:

$$\gamma_{BOND}^{AB} - 0.85(\gamma_{S,o}^{A} + \gamma_{S,o}^{B}) = \gamma_{SS}^{CHEM} \qquad (12)$$

This final form of the equation relates the electronic properties of the solids (included in the term γ_{SS}^{CHEM}) to the bond strength.

For the case of a liquid infiltrant in contact with a solid media, an analagous approach to the solid-solid case is presented which relates the work of adhesion to the interfacial tensions and wettability at the solid-liquid interface.

The work of adhesion for a pure liquid metal (A) in contact with a pure solid substrate (B) is defined as: $W_{SL} = \gamma^{B}_{SL} + \gamma^{B}_{SL} - \gamma^{B}_{SL}$, where W_{sl} is the work of adhesion, and the subscripts S,L, and V refer to solid, liquid, and vapor respectively. The difference between the definition of the work of adhesion for a solid-liquid case and a solid-solid case is a thermal strain term which incorporates the effect of differential cooling rates at the solid-liquid interface. To increase the work of adhesion then, γ^{B}_{SV} and γ^{A}_{LV} must be increased and γ^{AB}_{SL} decreased.

A strong bond may come at the expense of good wettability or liquid/solid contact angles during infiltration. According to the Young equation, as shown in Figure 14, to achieve good wettability or low contact angles, γ^{A}_{LV} must decrease or at least be smaller than the difference $\gamma^{B}_{SV} - \gamma^{AB}_{SL}$. Adding surface active elements to the liquid melt (alloying to reduce γ^{A}_{LV}) is one method to increase wettability. In the previous infiltration kinetics equation, infiltration height was directly related to the term $\gamma^{A}_{LV} \cos \theta$; as the product $\gamma^{A}_{LV} \cos \theta$ increased, the infiltration height increased. Also, for a constant γ^{A}_{LV}, the greater will be the bond strength as the contact angle, θ, is decreased; hence, another method to increase both wettability and bond strength simultaneously, is to increase γ^{B}_{SV} by coating or impregnating the solid metal surface. Coatings such as copper, nickel and tin are being used to improve the wetting of the silicon carbide.

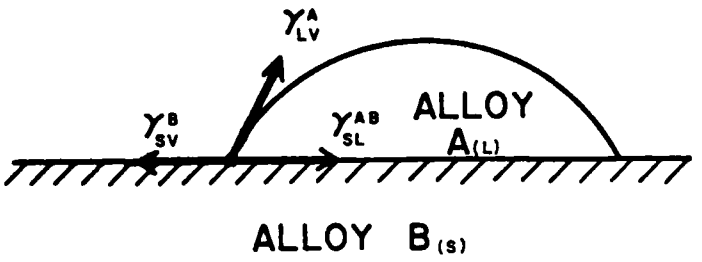

$$\gamma^A_{LV}\cos\theta = \gamma^B_{SV} - \gamma^{AB}_{SL}$$

Figure 14. Diagram of surface tension forces between a solid surface and a liquid drop.

A model was developed to predict or characterize the interaction between aluminum and silicon carbide in terms of bond strength and wettability and a brief outline of the model will be presented. Beginning with the Young equation, $\gamma_{LV}^{A}\cos\theta$ is equal to the difference between the solid-vapor interfacial tension γ_{SV}^{B} and the solid-liquid interfacial tension γ_{SL}^{AB}. According to Miedema, chemical interactions between dissimilar macroscopic surfaces can be treated in a way analogous to the treatment of the contact interactions between dissimilar atoms. The interfacial energy between solid (B) and liquid (A), γ_{SL}^{AB}, is described by the following expression:

$$\gamma_{SL}^{AB} = (\gamma_{SL}^{'})_B + (\gamma_{SL}^{''})_A + \gamma_{SL}^{'''} \qquad (14)$$

The first term $(\gamma_{SL}^{'})_B$ is an enthalpy term for the atoms in the first atomic layer of the solid in contact with the melt; this enthalpy change is a fixed fraction of the latent heat and considers only nearest neighbor interactions.

The second term $(\gamma_{SL}^{''})_A$ is related to the decrease in entropy of the first layer of liquid (A) atoms in contact with an inpenetratable, rigid solid (B) surface; this term is the interfacial excess entropy of liquid A. All interaction effects between A and B atoms are included in the third term, $\gamma_{SL}^{'''}$, the chemical interaction term. It is assumed that this chemical term is the same for the case of an isolated atom A present in a matrix of metal B (or vice versa) and a macroscopic droplet of metal A in contact with metal B. The term $\gamma_{SL}^{'''}$ is proportional to the enthalpy of solution, which, according to Miedema, is given by:

$$\Delta H_f \sim [-Pe(\Delta\phi^{*})^{2} + Q_o\,(\Delta n_{ws}^{1/3})^{2} - R]$$

The term γ_{SV}^{B} has also been semi-empirically modeled by Miedema, and is related to the contact potential (or work function) by the expression:

$$\gamma_{SV}^{B} = \eta_{ws}^{5/3} (\phi^{*} - 0.6)^{2} + DT \qquad (15)$$

where:

D is a constant

Combining the above expressions for both γ_{SV}^{B} and γ_{SL}^{AB} illustrates that the γ_{LV}^{A} cosθ term is related to a number of physical properties, as shown in the following expression:

$$\gamma_{LV}^{A}\cos\theta = [\eta_{ws}^{5/3} (\phi^{*}-0.6)^{2} + DT]-[AL_{f} + BS^{*} + C[-Pe(\Delta\phi^{*})^{2} + Q_{o} (\Delta\eta_{ws}^{1/3})^{2} - R]] \qquad (16)$$

In general then, to increase γ_{LV}^{A} cosθ:

1) Decrease ΔH of formation or increase $\Delta\Phi^{*}$ (i.e. chemical interaction should increase both infiltration rate and bond strength).
2) Increase temperature.
3) Increase Φ^{*} (work function) of the solid substrate (i.e. impregnate or coat the solid substrate) or decrease the latent heat of fusion.
4) Decrease the change in entropy at the surface by adding components which will lower the liquid surface tension.

Preliminary Experiments

Initial attempts were made to infiltrate a packed column of 0.5-10μm SiC powder (using distilled water as a binder) with pure molten aluminum. As shown previously, there was evidence to indicate that, if the temperature of the molten aluminum in contact with SiC was greater than 950C, then the contact angle would drop below 90° and the aluminum would wet the SiC particles. However, pure molten aluminum did not wet or infiltrate a packed SiC column, even after a number of attempts to minimize any type of impurity or contaminant (i.e. oxides, trace elements, etc.). As a result, experiments were begun to increase wettability by coating or impregnating the surface of the SiC solid.

Electroless copper, nickel, and tin will all be used to enhance the wettability of the silicon carbide surface. All of these metals should lower the contact angle between molten aluminum and silicon carbide. Because silicon carbide is a semiconductor and also oxidizes to form SiO_2, it is difficult to use conventional electroplating techniques. In addition, electroplating silicon carbide particles uniformly is a difficult process.

A procedure has been developed which will reproducibly coat SiC with electroless metals; this procedure has been used to successfully coat SiC particles with copper. The procedure is as follows:

1) Sensitization of the SiC powder with a 10ml/l $SnCl_2$ and 40ml/l HCl solution at 30C.
2) Activation of the surface with a $PdCl_2$ solution (30C).
3) Repeat of steps 1) and 2).
4) Coating of the particles with a two-part electroless plating solution supplied by Copper Technology Corporation (10% CT 400A and 10% CT 400B)

SEM (Scanning Electron Microscope) micrographs of the copper coated silicon carbide particles are shown in the attached micrographs (Figure 15(a) and (b)). Although not all of the particles were covered, the observed coating cannot be easily rubbed off (coatings are typically baked onto the surface at higher temperatures to improve adhesion). Another micrograph, Figure 15(c), shows the fine particulate form of the stannous chloride on the surface of a silicon carbide particle.

We are currently attempting to prepare packed columns of these metal-coated SiC particles, then infiltrate the compact with molten aluminum.

ACKNOWLEDGEMENTS

The authors acknowledge, with appreciation, the research support of the Office of Naval Research. The support and interest of Dr. Steven Fishman has been greatly appreciated.

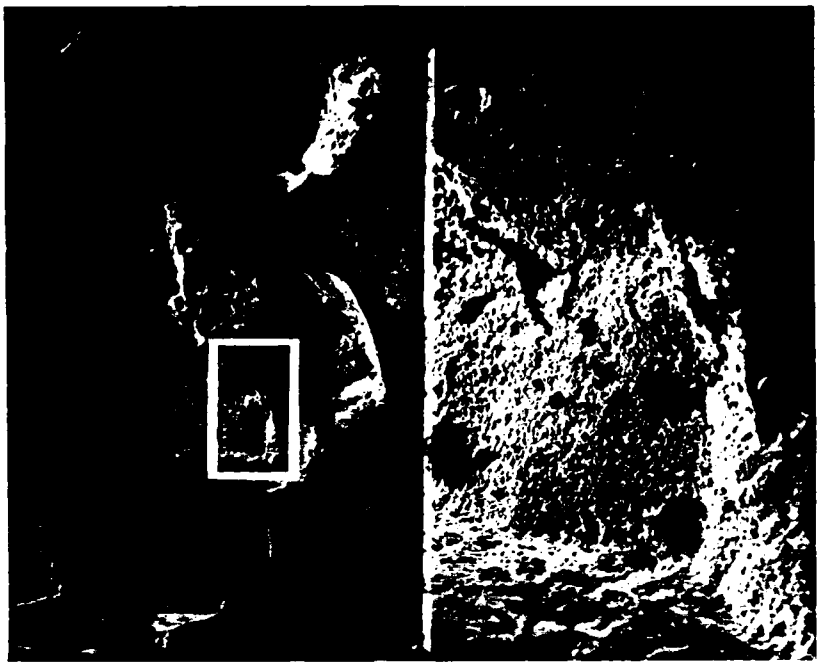

a)

b) c)

Figure 15. Electroless copper coated SiC particles a) and b): SEM micrographs of coatings (Mag. 400) c) $SnCl_2$ particulates on SiC particles (Mag. 1700).

LIST OF FIGURES

END

DTIC

9-86